RSC Advances

ROYAL SOCIETY OF CHEMISTRY

www.rsc.org/advances

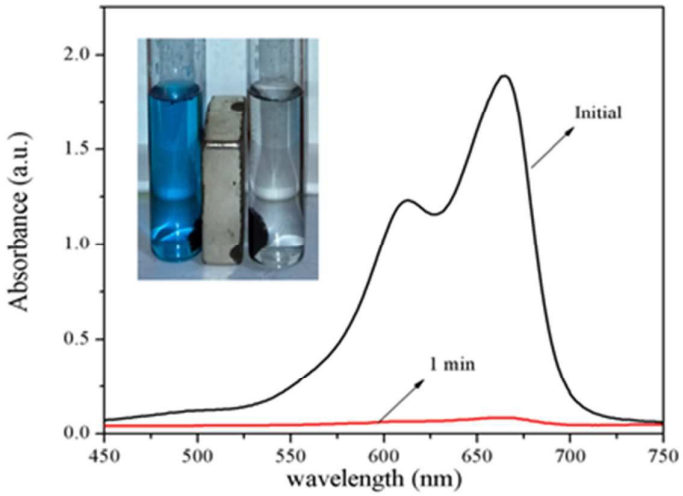

Hierarchical magnetic porous carbon fibers (MBFs) were fabricated by annealing Fe(BTC)-coated bamboo fibers, which were produced using a new synthesis route for growing Fe(BTC) on bamboo fiber materials in nitrogen atmosphere. Results demonstrated that the obtained hybrid materials possess high adsorption capacity and can be easily recycled from liquid media by using an external magnetic field. MBF adsorption reached equilibrium within approximately 1 min and the adsorption capacity rapidly reached 143 mg/g.

Self-template synthesis of hierarchical magnetic porous carbon fibers derived from Fe(BTC)-coated bamboo fibers for fast removal of methylene blue

Chao Bao[1a], Junjun Ma[1a], Lincheng Zhou[*a], Yanming Shao[a], Qiong Wu[a], Fei Wang[b]

[a]*State Key Laboratory of Applied Organic Chemistry, College of Chemistry and Chemical Engineering, Institute of Biochemical Engineering & Environmental Technology, Lanzhou University, Lanzhou 730000, P. R. China*

[b]*Changjiang Engineering Supervison Consulting Co. Ltd, Wuhan 430010, P. R. China*

Chao Bao E-mail: baoch13@lzu.edu.cn Fax: 86-931-8912113 Tel. 86-931-8912528

Address: College of Chemistry and Chemical Engineering, Lanzhou University, Lanzhou 730000, P.R.China

Junjun Ma E-mail: majj12@lzu.edu.cn Fax: 86-931-8912113 Tel. 86-931-8912528

Address: College of Chemistry and Chemical Engineering, Lanzhou University, Lanzhou 730000, P.R.China

Lincheng Zhou E-mail: zhoulc@lzu.edu.cn Fax: 86-931-8912113 Tel. 86-931-8912528

Address: College of Chemistry and Chemical Engineering, Lanzhou University, Lanzhou 730000, P.R.China

Yanming Shao E-mail: shaoym11@lzu.edu.cn Fax: 86-931-8912113 Tel. 86-931-8912528

Address: College of Chemistry and Chemical Engineering, Lanzhou University, Lanzhou 730000, P.R.China

Qiong Wu E-mail: qwu14@lzu.edu.cn Fax: 86-931-8912113 Tel. 86-931-8912528

Address: College of Chemistry and Chemical Engineering, Lanzhou University, Lanzhou 730000, P.R.China

Fei Wang E-mail: 41103045@qq.com Fax: 86-931-8912113 Tel. 86-931-8912528

Address: Changjiang Engineering Supervison Consulting Co. Ltd, Wuhan 430010, P.R.China

[*]Corresponding author. Tel: 86-931-8912528. E-mail: Zhoulc@lzu.edu.cn (Zhou lincheng)
[1]These authors contributed equally to this work.

Abstract

Hierarchical magnetic porous carbon fibers (MBFs) were fabricated by annealing Fe(BTC)-coated bamboo fibers, which were produced using a new synthesis route for growing Fe(BTC) on bamboo fiber materials, in nitrogen atmosphere. The materials were characterized using scanning electron microscopy, X-ray diffraction, X-ray photoelectron spectroscopy, Mössbauer spectroscopy, Brunauer–Emmett–Teller surface area measurement, and vibrating sample magnetometry. The obtained MBF composites possess both high surface areas and magnetic characteristics. Their adsorption properties were preliminarily tested by the adsorptive removal of methylene blue from aqueous solution. Results demonstrated that the obtained hybrid materials possess high adsorption capacity and can be easily recycled from liquid media by using an external magnetic field. MBF adsorption reached equilibrium within approximately 1 min and the adsorption capacity rapidly reached 143 mg/g. Most importantly, MBF can be reused after washing with ethanol. After six reuses, the removal efficiency could still reach 80%. Moreover, the low-cost raw material used (i.e., bamboo) is abundant and renewable. This study indicated that the as-prepared MBF composites show great potential for use in a wide range of applications.

1. Introduction

Industry dyes and pigments are becoming ubiquitous sources of environmental pollution because of their carcinogenic and mutagenic effects on aquatic organisms.[1] In the past few decades, several technologies, such as chemical oxidation, biological treatment, ion exchange, and membrane separation, have been developed to remove environmental pollutants.[2-4] Adsorption is a simple and efficient technique in removing different types of coloring materials from water because of its excellent treatment effect.[5] Many types of adsorbents, including activated carbon,[6, 7] biopolymers, clay materials,[8] and zeolites,[9] have been given significant research interest in recent years. Among the numerous types of adsorbents, activated carbon is the most widely used because of its robust porous networks and superior characteristics, including lightweight and environmentally friendly. However, commercially available activated carbon is becoming too expensive. In the last few years, special emphasis has been placed on the preparation of activated carbons from several agricultural byproducts because of the growing interest in low-cost activated carbons from renewable sources, especially for application in wastewater treatment. Researchers studied the production of activated carbon from coconut shells,[10] oil palm fiber,[11] date stones,[12] and rubber seed coat.[13]

Metal–organic frameworks (MOFs) are crystalline materials composed of metal ions and organic ligands. The pore size and functional groups of MOFs can be adjusted given the enormous variety of metal ions and organic ligands.[14] In addition, MOFs are excellent candidates for various applications, such as gas adsorption and storage,[15-17] biomedicine and drug delivery,[18, 19] separation[20-22] and adsorption of organic molecules,[23-25] as well as sensing,[26] magnetism,[27] and nanomaterial carriers[28], because of their large surface area,

tunable pore size, and modifiable unsaturated or saturated metal sites. MOFs have also been used as adsorbent. However, the low stability of MOFs limits their application in special environments, such as acid, alkali, and high temperature. MOFs are used as templates or precursor materials to produce porous carbonaceous materials because they have large surface area and a significant amount of carbon.[29]

Bamboo, which is a member of the most diverse group of plants in the grass family, is an enduring, versatile, highly renewable, and abundant natural resource in China because it takes only a few months to grow to maturity. Bamboo is used in constructing various living facilities and tools.[30] Bamboo is also used for furniture-making and construction because it is inexpensive, strong, tough, and longer than other hardwoods. Conversion of bamboo to a value-added product such as activated carbon will help solve part of the problem of wastewater treatment. The advantage of using agricultural byproducts as raw materials for preparing activated carbon is that these raw materials are abundant, renewable, and potentially less expensive. However, separating porous carbon from aqueous solution is difficult, thus limiting their applications in this field. Introduction of magnetic particles into porous carbon can enlarge the scope of applications.[31-33]

In this paper, hierarchical magnetic porous carbon fibers (MBFs) were prepared by annealing Fe(BTC)-coated bamboo fibers (BFs), which were fabricated by a new route for growing MOFs on BFs, in nitrogen atmosphere. First, the BFs were modified using chloroacetic acid. Subsequently, Fe(BTC)-coated BFs were prepared using the modified BFs as templates through a self-template synthesis strategy. Finally, MBFs were fabricated by annealing Fe(BTC)-coated BFs in nitrogen atmosphere under different temperature. The

as-prepared magnetic composites were characterized using scanning electron microscopy (SEM), X-ray diffraction, X-ray photon spectroscopy (XPS), vibrating sample magnetometry (VSM), and Brunauer–Emmett–Teller (BET) surface area measurement. MBF was used as an adsorbent to remove a cationic dye methylene blue (MB) from water. We investigated the effect of carbonization temperature and adsorption isotherms of MB on the hierarchical MBFs. The as-synthesized MBFs showed high efficiency in magnetic separation and recovery owing to high-saturation magnetization. Thus, MBFs are excellent absorbents for practical applications.

2. Experimental

2.1 Materials

$FeCl_3$ and chloroacetic acid ($ClCH_2COOH$) were purchased from Sinopharm Chemical Reagent Co. (Shanghai,China). Benzene-1,3,5-tricarboxylicacid (H_3BTC) and H_2SO_4 were purchased from Aldrich. Sodium hydroxide (NaOH) was purchased from Shanghai Chemical Reagents Company. Methylene blue (MB) was supplied by Tianjin Tiantai Fine Chemicals Co., Ltd. All the chemicals were of analytical grade.

2.2 Preparation of the MBFs

Raw material (bamboo) was collected from a local furniture shop and then washed with ultrapure water and ethanol for several times to remove dust-like impurities. The bamboo was then dried under vacuum at 100 °C, ground, and sieved to certain sizes for further use.

First, the BFs were modified using chloroacetic acid to activate the raw material. In a typical experiment, raw material was impregnated by mixed solution (pH = 9) of NaOH and $ClCH_2COOH$ with stirring for 24 h at 40 °C. BFs were then obtained by filtration and

repeatedly washed with ultrapure water to remove residual NaOH and $ClCH_2COOH$. Products were collected and soaked in ethanol solution of saturated ferric chloride for 10 h at 78 ℃. Then, the products were washed with ultrapure water and sealed in a Teflon-lined stainless steel autoclave with ethanol solution of saturated H_3BTC for 10 h at 78 °C. The as-prepared products were washed with ethanol solution and dried for further use. Finally, MBF-500, MBF-700, and MBF-900 were prepared by annealing the products at 500, 700, and 900 ℃, respectively, in nitrogen atmosphere for 1 h. The as-prepared products were collected after cooling to room temperature.

2.3 Adsorption experiment

The as-prepared MBFs were evaluated as an adsorbent by choosing MB as a model molecule. First, an aqueous stock solution of MB (1000 $mg \cdot L^{-1}$) was prepared by dissolving MB in deionized water. Aqueous MB solutions with different concentrations (0-400 $mg \cdot L^{-1}$) were then prepared by successive dilution of the stock solution with deionized water. An exact amount of the MBFs composite (10 mg) was added to the MB solutions (10 mL) at different concentrations. The conical flask containing the solution was fixed on a shaker at 30ºC, and the decay of MB concentrations versus contact time was measured by UV-Vis spectroscopy (Purkinje General) at 664 nm at various intervals. The amount of MB adsorbed per unit mass of the adsorbent (Q_e in mg g^{-1}) was evaluated by $Q_e = \frac{(C_o - C_t)V}{m}$ (1)

Where C_o and C_t are the initial and equilibrium concentrations of MB (mg L^{-1}), respectively, m is the weight of the adsorbent used (g), and V is the volume of the aqueous solution (L). The adsorption kinetic study was carried out following the above adsorption procedure at certain intervals of time with 10 mL solutions (60 mg L^{-1}). The effect of MB

concentration was studied over a MB concentration range of 10-80 mg/L. The progress of the conversion reaction was monitored by measuring the changes in absorbance at 664 nm with a UV-vis spectrophotometer.

2.4 Desorption experiments

Solvent desorption technique was used to evaluate the feasibility of regenerating the MB-saturated MBFs. Solutions of ethanol with HCl (1.0%, v/v) were tested as the eluent to regenerate MBFs. An eluent solution (10 mL) was added to the used MBFs and the mixture was ultrasonicated for 30 min. The adsorbent was separated from the solution by using an external magnetic field and then dried at 50 °C.

2.5 Stability Tests

The recyclability of MBF-900 for MB reduction was also investigated for six cycles. After each run, solid composites were recovered with a magnet, washed with water and ethanol, and dried under vacuum. To evaluate stability, MB concentration was determined via UV–vis detection of residual MB in the mixture after reaction.

2.6 Characterization

FT-IR spectra were obtained in transmission mode on a FT-IR spectrometer (American Nicolet Corp., Model 170-SX) using the KBr pellet technique. Sample morphology was examined using a scanning electron microscope (SEM, JSM-6701F, JEOL, Japan). Magnetization measurements at room temperature were obtained using a Vibrating sample magnetometer (LAKESHORE-7304, USA) at room temperature. The X-ray photoelectron spectroscopy (XPS) spectra were obtained with an ESCALab220i-XL electron spectrometer (VG Scientific) using 300 W Al-K_{α} radiation. The velocity calibration at room temperature

(RT) was performed using an α-Fe absorber, and the isomer shift (IS) values reported are relative to α-Fe. The N_2 adsorption-desorption isotherm was measured at liquid nitrogen temperature (77 K) using a Micromeritics ASAP 2020 analyzer. The specific surface area was calculated by the BET method. The pore size distribution was obtained using the Barret-Joner-Halenda (BJH) method. UV-Vis detection was carried out on a TU-1810PC UV-Vis spectrophotometer (Purkinje General, China).

3. Results and discussion

3.1 Morphology and structure characterization

The procedure for the synthesis of MBFs in the present work is illustrated in Fig. 1. First, the BFs were modified using chloroacetic acid to activate the raw material. Then, BF–Fe(BTC) composites were obtained using a self-template strategy. Finally, MBF-500, MBF-700, and MBF-900 were prepared by annealing the products at 500 °C, 700 °C, and 900 °C, respectively. Fig. 2 shows representative SEM images of BFs (Figs. 2a, 2b), BF–COOH (Figs. 2c, 2d), BF–COOH–Fe^{3+} (Figs. 2e, 2f), and BF–Fe(BTC) (Figs. 2g, 2h). The surface of BFs were extremely smooth (Figs. 2a, 2b), but it became rougher after the modifications [Figs. 2(c–h)]. The result indicates that the modification of BFs was successful.

The thermal stability of BF–Fe(BTC) was studied using TGA under an inert atmosphere. Fig. S1 presents typical TGA curves of the BFs and BF–Fe(BTC) composite. TGA curve shows both BFs and BF–Fe(BTC) composite exhibit a slope between 30 °C and 100 °C, which may be caused by the loss of H_2O. Moreover, the TGA curves of BF and BF–Fe(BTC) composites exhibit a steep slope between 300 and 450 °C and between 300 and 500 °C, respectively, which indicate approximately 75% and 70% weight losses because of

decomposition (i.e., production of residual carbon). These results provided a reference for selecting the appropriate carbonization temperature.

SEM images of unmodified CBF (Figs. 3a, 3b), MBF-500 (Figs. 3c, 3d), MBF-700 (Figs. 3e, 3f), and MBF-900 (Figs. 3g, 3h) revealed that the composite materials retained their shapes. As shown in Fig. 3, the surfaces of MBF-500, MBF-700, and MBF-900 were rougher than that of CBF, indicating that the BFs were modified. What is more, For MBF-t, the surface appeared to rougher with increasing annealing temperature.

The composition of the resulting hybrid magnetic microspheres was verified using XPS by investigating the chemical state of the surface of obtained MBF-900. Fig. 4a shows the overall surveys of the as-synthesized MBF-900, which clearly show the signals of elemental C, O, and Fe. Fig. 4b shows the XPS spectrum of Fe 2p. The Fe 2p spectrum can be deconvoluted into two peaks centered at 725.3 and 711.2 eV, which correspond to the peaks of Fe $2p_{1/2}$ and Fe $2p_{3/2}$, respectively. Meanwhile, the Fe $2p_{3/2}$ spectrum was resolved into two peaks at 710.64 and 712.17 eV, which correspond to Fe^{2+} and Fe^{3+}. In addition, the signal at 720.46 eV is characteristic of γ-Fe_2O_3; this signal is not obvious in Fe_3O_4.[34] Fig. 4c shows the XPS spectra of C 1s, which can be deconvoluted into three peaks centered at 283.0, 284.5, and 285.1 eV that correspond to FeC_3, C=O, and C–C/C=C species, respectively.[35] Fig. 4d shows the XPS spectra of O 1s, which can be deconvoluted into three peaks centered at 530.7, 532.5, and 533.2 eV that respectively correspond to C=O, Fe–O and O–C=O species. These results also confirm that the BFs were successfully modified.

The ^{57}Fe Mössbauer spectra for the MBFs are presented in Fig. 5. A central single peak was detected, which most possibly reflects the interface phase between carbon and Fe_3O_4 in

the MBF-500 (Fig.5a).[2, 36] The presence of doublets can be observed in Figs. 5b and 5c, suggesting the formation and dispersion of small-particle iron oxides over carbons fiber. Besides, sextets with IS = 0.20 mms^{-1} are related to Fe_3C.[37] The peak area in the Mössbauer spectrum suggests the content of major iron phases. As carbonize temperature increased, the ratio of the reduction reactions between iron oxide and carbon increased, and the ratio of Fe_3C increased as well. The high ratio of Fe–C decided the stability between iron and carbon fiber, which is beneficial for recycling.

The BET surface area was measured from the N_2 adsorption/desorption isotherms at −197.2 °C. Prior to measurements, the samples were evacuated at 100 °C for 10 h. The BET surface areas of MBF-500, MBF-700, and MBF-900 were 359.33, 360.72, and 387.74 m^2/g, respectively (Fig. 6). The data are summarized in Table 1. For MBF-t, the specific surface area appeared to increase with increasing annealing temperature. This may be due to high temperature produces a positive effect in producing H_2O and CO_2, which could expand pore size. The pore-size distribution curves of MBF-500, MBF-700, and MBF-900 were estimated from the desorption curves of the isotherm using BJH analyses. The figures show that the pore size distribution curve of MBF-500, MBF-700, and MBF-900 were 2.66, 2.69, and 3.50 nm, respectively. The high BET surface areas and pore size of the MBF-t should be useful for MB removal by increasing the contact frequency between the MB and MBF-t.

The magnetic properties of the resultant core-shell microspheres were investigated at room temperature using VSM in the field range of −10 kOe to 10 kOe (Fig. 7). The magnetization saturation values of C(BF–$FeCl_3$)-900, MBF-500, MBF-700, and MBF-900 were 6.2, 7.1, 8.4, and 9.8 emu/g, respectively. Measured values indicated the strong magnetic

properties of MBF-t. All of the curves present a magnetic hysteresis loop that confirms the strong magnetic response to a varying magnetic field. Saturation magnetization values appeared to increase with increasing annealing temperature. Coercivity and remanence values are summarized in Table 2. Fast aggregation of nanocatalysts can be observed from their homogeneous dispersion in the presence of an external magnetic field applied for 30 s. This observation directly demonstrates the convenient separation of MBF-t through an external magnetic field, which is important in terms of their practical manipulation.

3.2 Adsorption properties of MBFs

3.2.1 Adsorption kinetics

To compare the adsorption efficiency of MBF-500, MBF-700, and MBF-900, the effect of connect time on the adsorption of MB onto MBF composites was first investigated by adding 10 mg sample to 10 mL MB solution. After shaking for predetermined time interval, the magnetic particles were magnetically separated. Then, the corresponding dye concentrations in the solutions were measured using UV–vis spectrometry. The adsorption capacity increased rapidly and reached the adsorption equilibrium within 2 min (Fig. 8), implying that the MBF-900 magnetic composite possesses both higher adsorption capacity and higher adsorption efficiency for the removal of pollutants from water compared with other carbon materials. Result also indicated the increase in adsorption capacity with increasing annealing temperature, which corresponded to the BET surface area analysis. From the results, the removal efficiency of MBF-900 for MB was excellent and it was selected as an adsorbent for MB. In order to analyze the adsorption kinetics of MBF-900, four kinetic models including the pseudo-first-order equation,[38] the pseudo-second-order equation,[39]

Elovich equation,[40] and intraparticle diffusion model[41] were applied to experimental data obtained from removal experiments. A pseudo-first-order kinetic model of Lagergen is given as log (Q_e-Q_t) = log Q_e −K_1t/2.303 (2)

A pseudo-second-order kinetic model is

$$\frac{t}{Q_t} = \frac{1}{K_2 Q_e^2} + \frac{t}{Q_e} \quad (3)$$

an intraparticle diffusion model is

$$Q_t = K_3 t^{1/2} + C \quad (4)$$

And an Elovich equation model is shown as

$$Q_t = \ln(\alpha\beta)/\beta + \ln t/\beta \quad (5)$$

where Q_e and Q_t are the adsorption capacity (mg g^{-1}) at equilibrium time and at time t, respectively, and K_1 the pseudo-first-order rate constant for the adsorption process (min^{-1}). K_2 the rate constant of pseudo-second-order adsorption (g mg^{-1} min^{-1}). K_3 the intraparticle diffusion rate constant (mg g^{-1} min^{-1}). C the intercept, α the initial sorption rate of Elovich equation (mg g^{-1} min^{-1}) the parameter β is related to the extent of surface coverage and activation energy for chemisorption (g mg^{-1}).The slopes and the intercepts of each linear plot are used to calculate the kinetic parameters for MB adsorption. As shown in Table 3, the pseudo-second-order kinetic curves give a good fit to the experimental kinetic data, and the high correlation coefficient (R^2 > 0.97) indicated typical chemical adsorption.[42] The rate constant, k, of MB absorption is calculated as 5.54 s^{-1} for the case of MBF-900, which is much larger than other nanoadsorbents, including magnetic Fe_3O_4@carbon nanofibers,[43] sphere-like $SrCO_3$ nanostructures,[44] and Cu_2O@reduced grapheme oxide composites.[45] MB is an ideally planar molecule; therefore, it can be adsorbed easily by p–p stacking interactions

between the aromatic backbone of the dye and the hexagonal skeleton of the carbon shell.[46] Adsorption progressed with MB molecules first adsorbing onto the surface of MBF-900. MB was adsorbed onto the surface of MBF-900 through electrostatic attraction because MB is a cationic dye and some carboxylate groups derived from H_3BTC exist on the surface of MBF-900. MB then diffused into the cavity through the channel of the porous. Finally, the result was confirmed from the shift in the adsorption peak of the carboxylate groups from 1448 cm^{-1} to 1408 cm^{-1} (Fig. S2).

3.2.2 Adsorption isotherms

The uptake of MB on MBF-900 was investigated at 298 K. As shown in Fig. 10a, adsorption isotherms describe the distribution of adsorbate molecules between the liquid phase and the solid phase. The Langmuir (Eq. 6), Freundlich (Eq. 7), and Temkin (Eq. 8) models are often used to describe equilibrium sorption isotherm. The equation parameters and the underlying thermodynamic assumptions of these equilibrium models often provide some insight into both the sorption mechanisms and the surface properties and affinities of the adsorbent. These models were the conventional adsorption isotherm models employed in this study to describe MB adsorption equilibrium.[47] The Langmuir model, which is valid for monolayer adsorption onto a surface containing a finite number of identical sites, is probably the most popular isotherm model due to its simplicity and its good agreement with experimental data. It could be described by the linearized form:

$$\frac{C_e}{Q_e} = \frac{1}{Q_m K_L} + \frac{C_e}{Q_m} \qquad (6)$$

Where Q_{max} is the maximum adsorption capacity and K_L is the adsorption equilibrium constant including the affinity of binding sites (L mg^{-1}), Q_e is the adsorption capacity (mg g^{-1})

at equilibrium, C_e is the equilibrium concentration of the adsorbate (mg L^{-1}).

According to the Freundlich equation, the amount of substance adsorbed per gram of adsorbent (Qe) is related to the equilibrium concentration (C_e) by the equation as follows:

$$\ln Q_e = \ln K_F + \frac{1}{n} \ln C_e \quad (7)$$

Q_e is the adsorption capacity (mg g^{-1}) at equilibrium, C_e is the equilibrium concentration of the adsorbate (mg L^{-1}). K_F is the constant indicative of the relative adsorption capacity of the adsorbent (mg g^{-1}) and $1/n$ is the constant indicative of the intensity of the adsorption.

The Temkin isotherm equation describes the behavior of many adsorption systems on heterogeneous surface and it is based on the following equation:

$$Q_e = RT \ln(a_t C_e)/b_t \quad (8)$$

The linear form of Temkin isotherm can be expressed by Eq. (8):

$$Q_e = A + B \ln C_e \quad (9)$$

where Q_e is the adsorption capacity (mg g^{-1}) at equilibrium, C_e is the equilibrium concentration of the adsorbate (mg L^{-1}). R is the general gas constant, T absolute temperature (K), $A = (RT/b_t \ln a_t)$ and $B = (RT/b_t)$ represents isotherm constants, respectively. The values of K_F (mg$^{1-1/n}$ $L^{1/n}$ g^{-1}) and n can be calculated from the intercept and slope of the linearized plot of log Q_e vs. log C_e. The adsorption constant and the calculated regression coefficients (R^2) of the Langmuir, Freundlich, and Temkin at 298 K are summarized in Table 4. The Langmuir isotherm provided much higher R^2 values than did the Freundlich and Temkin isotherm for the adsorption of MB onto MBF-900 at 298 K, indicating that the Langmuir isotherm has better fit with the experimental data. The formation of monolayer coverage of MB molecules at the outer surface of the MBF-900 magnetic composites could be explained

by the homogeneous distribution of active site on the surface of the MBF-900 magnetic composites. The maximum monolayer adsorption capacity (Q_{max}) of MB was calculated to be 143.0 mg g^{-1} at 298 K, which was higher than previously reported adsorbents to remove MB (Table 5).[48-52]

3.2.3 Effect of MB concentration

The influence of MB dosage was investigated using the MB at 10, 20, 40, 60, and 80 mg L^{-1} (Fig. S3). As shown in Fig. S3, the removal efficiency of MB did not change significantly from 10 mg L^{-1} to 40 mg L^{-1}. The removal efficiency achieved was nearly 100% after 1 min of absorption. However, the efficiency decreased when MB concentration was too high. Removal efficiency still could reach 88% within 1 min when the concentration of MB was as high as 80 mg L^{-1}. Results indicated that the as-prepared MBF-900 possesses wonderful removal efficiency of MB.

3.3 Desorption and regeneration of MBF-900

The progress of MB adsorption can be easily followed by the decrease in absorbance at λ_{max} (664 nm) of MB with time. Fig. 11a shows the successive UV–vis detection of MB in the presence of MBF-900 in aqueous solution. Adsorption bead decreased rapidly and disappeared within 1 min without the appearance of new adsorption bands in the visible or ultraviolet regions, indicating that MB was almost removed completely. The inset demonstrates that MBF-900 could be separated from MB solution by a magnet within 30 s.

The regeneration of an adsorbent is important because of its commercial feasibility and may reduce the overall cost of the adsorbent. Desorption experiments were performed to evaluate the possibility of regeneration and reusability of MBF-900 as an adsorbent.

Desorption and regeneration experiments were achieved using ethanol (1% HCl). Used MBF-900 could be regenerated effectively by using ethanol with 1% HCl. The results of five consecutive adsorption–desorption cycles are shown in Fig. 11b. The adsorption capacity of MB on MBF-900 decreases as the cycle number increased. After six cycles, MB adsorption capacity is still above 80% of the first adsorption, showing that MBF-900 has higher adsorption capacity and can be recycled.

4 Conclusion

The present study revealed that BFs are promising precursor in preparing activated carbon. We demonstrated a feasible route to synthesize an ideal adsorbent that possessed both high specific surface area and sensitive magnetic characteristics. Most importantly, the as-prepared adsorbent is suitable for the removal of cationic dyes and metals ions in water owing to its abundant unsaturated carboxyl and channels. Unlike conventional adsorbents, the as-prepared magnetic MBF-900 porous adsorbent not only exhibited higher adsorption capacity, but it can also be separated easily from aqueous medium by using an external magnetic field and can be used repeatedly after washing with ethanol. Adsorption experiment demonstrated that the as-prepared magnetic MBF-900 exhibit a good adsorption performance for MB. The maximum adsorption can reach 143.0 mg g^{-1}. Therefore, the as-prepared composite shows a great potential for industrial application.

Acknowledgement

The authors would like to express their appreciation for research funding provided by the National Natural Science Foundation of China (Nos. 21374045, 21074049) and the National Science Foundation for Fostering Talents in Basic Research of the National Natural Science

Foundation of China (Grant No. J1103307).

References

1. H. Demir, A. Top, D. Balköse and S. Ülkü, *Journal of Hazardous Materials*, 2008, **153**, 389-394.
2. L. Zhou, Y. Shao, J. Liu, Z. Ye, H. Zhang, J. Ma, Y. Jia, W. Gao and Y. Li, *ACS Applied Materials & Interfaces*, 2014, **6**, 7275-7285.
3. Y. Zhang, Y. Xiong, Y. Tang and Y. Wang, *Journal of Hazardous Materials*, 2013, **244–245**, 758-764.
4. P. S. Bäuerlein, T. L. ter Laak, R. C. H. M. Hofman-Caris, P. de Voogt and S. T. J. Droge, *Water Research*, 2012, **46**, 5009-5018.
5. M. Rafatullah, O. Sulaiman, R. Hashim and A. Ahmad, *Journal of Hazardous Materials*, 2010, **177**, 70-80.
6. Z. Hu, M. P. Srinivasan and Y. Ni, *Carbon*, 2001, **39**, 877-886.
7. Z. Hu and M. P. Srinivasan, *Microporous and Mesoporous Materials*, 2001, **43**, 267-275.
8. G. Crini, *Bioresource Technology*, 2006, **97**, 1061-1085.
9. J. Yang, Y. Zhou, J. Y. Yang, W. G. Lin, Y. J. Wu, N. Lin, J. Wang and J. H. Zhu, *The Journal of Physical Chemistry C*, 2010, **114**, 9588-9595.
10. K. P. Singh, A. Malik, S. Sinha and P. Ojha, *Journal of Hazardous Materials*, 2008, **150**, 626-641.
11. I. A. W. Tan, B. H. Hameed and A. L. Ahmad, *Chemical Engineering Journal*, 2007, **127**, 111-119.
12. B. H. Hameed, J. M. Salman and A. L. Ahmad, *Journal of Hazardous Materials*, 2009, **163**, 121-126.
13. S. Rengaraj, S.-H. Moon, R. Sivabalan, B. Arabindoo and V. Murugesan, *Journal of Hazardous Materials*, 2002, **89**, 185-196.
14. J. Park, Z. U. Wang, L.-B. Sun, Y.-P. Chen and H.-C. Zhou, *Journal of the American Chemical Society*, 2012, **134**, 20110-20116.
15. B. Chen, N. W. Ockwig, A. R. Millward, D. S. Contreras and O. M. Yaghi, *Angew Chem Int Ed Engl*, 2005, **44**, 4745-4749.
16. M. Dincă and J. R. Long, *Journal of the American Chemical Society*, 2005, **127**, 9376-9377.
17. H. Chun, D. N. Dybtsev, H. Kim and K. Kim, *Chemistry*, 2005, **11**, 3521-3529.
18. P. Horcajada, R. Gref, T. Baati, P. K. Allan, G. Maurin, P. Couvreur, G. Férey, R. E. Morris and C. Serre, *Chemical Reviews*, 2011, **112**, 1232-1268.
19. P. Horcajada, C. Serre, M. Vallet-Regi, M. Sebban, F. Taulelle and G. Ferey, *Angew Chem Int Ed Engl*, 2006, **45**, 5974-5978.
20. J.-R. Li, J. Sculley and H.-C. Zhou, *Chemical Reviews*, 2011, **112**, 869-932.
21. J. R. Li, R. J. Kuppler and H. C. Zhou, *Chemical Society reviews*, 2009, **38**, 1477-1504.
22. R. Kitaura, K. Seki, G. Akiyama and S. Kitagawa, *Angewandte Chemie International Edition*, 2003, **42**, 428-431.
23. T. K. Trung, P. Trens, N. Tanchoux, S. Bourrelly, P. L. Llewellyn, S. Loera-Serna, C. Serre, T. Loiseau, F. Fajula and G. Férey, *Journal of the American Chemical Society*, 2008, **130**, 16926-16932.
24. X. Wang, L. Liu and A. J. Jacobson, *Angew Chem Int Ed Engl*, 2006, **45**, 6499-6503.
25. C. Chen, M. Zhang, Q. Guan and W. Li, *Chemical Engineering Journal*, 2012, **183**, 60-67.
26. O. K. Farha, A. Özgür Yazaydın, I. Eryazici, C. D. Malliakas, B. G. Hauser, M. G. Kanatzidis, S. T. Nguyen, R. Q. Snurr and J. T. Hupp, *Nat Chem*, 2010, **2**, 944-948.
27. D. Maspoch, D. Ruiz-Molina and J. Veciana, *Journal of Materials Chemistry*, 2004, **14**, 2713.
28. S. Hermes, F. Schröder, R. Chelmowski, C. Wöll and R. A. Fischer, *Journal of the American Chemical Society*, 2005, **127**, 13744-13745.

29. W. Cho, S. Park and M. Oh, *Chemical Communications*, 2011, **47**, 4138-4140.
30. F. G. Shin, X. J. Xian, W. P. Zheng and M. W. Yipp, *J Mater Sci*, 1989, **24**, 3483-3490.
31. T. Muraliganth, A. Vadivel Murugan and A. Manthiram, *Chemical Communications*, 2009, 7360-7362.
32. M. Baikousi, A. B. Bourlinos, A. Douvalis, T. Bakas, D. F. Anagnostopoulos, J. Tuček, K. Šafářová, R. Zboril and M. A. Karakassides, *Langmuir*, 2012, **28**, 3918-3930.
33. H. Wang, Y.-B. Sun, Q.-W. Chen, Y.-F. Yu and K. Cheng, *Dalton Transactions*, 2010, **39**, 9565-9569.
34. Z. Wu, W. Li, P. A. Webley and D. Zhao, *Advanced Materials*, 2012, **24**, 485-491.
35. M.-J. Jung, E. Jeong, S. Cho, S. Y. Yeo and Y.-S. Lee, *Journal of Colloid and Interface Science*, 2012, **381**, 152-157.
36. A. Banerjee, R. Gokhale, S. Bhatnagar, J. Jog, M. Bhardwaj, B. Lefez, B. Hannoyer and S. Ogale, *Journal of Materials Chemistry*, 2012, **22**, 19694-19699.
37. Z. H. Sun, L. F. Wang, P. P. Liu, S. C. Wang, B. Sun, D. Z. Jiang and F. S. Xiao, *Advanced Materials*, 2006, **18**, 1968-1971.
38. K. K. Panday, G. Prasad and V. N. Singh, *Water Research*, 1985, **19**, 869-873.
39. S. Rengaraj, Y. Kim, C. K. Joo and J. Yi, *Journal of Colloid and Interface Science*, 2004, **273**, 14-21.
40. F.-C. Wu, R.-L. Tseng and R.-S. Juang, *Journal of Hazardous Materials*, 2001, **81**, 167-177.
41. N. Chiron, R. Guilet and E. Deydier, *Water Research*, 2003, **37**, 3079-3086.
42. Y. Tan, M. Chen and Y. Hao, *Chemical Engineering Journal*, 2012, **191**, 104-111.
43. Y. Si, T. Ren, B. Ding, J. Yu and G. Sun, *Journal of Materials Chemistry*, 2012, **22**, 4619-4622.
44. S. Wu, S. Yin, H. Cao, Y. Lu, J. Yin and B. Li, *Journal of Materials Chemistry*, 2011, **21**, 8734-8741.
45. B. Li, H. Cao, G. Yin, Y. Lu and J. Yin, *Journal of Materials Chemistry*, 2011, **21**, 10645-10648.
46. S. Bai, X. Shen, X. Zhong, Y. Liu, G. Zhu, X. Xu and K. Chen, *Carbon*, 2012, **50**, 2337-2346.
47. B. H. Hameed and A. A. Rahman, *Journal of Hazardous Materials*, 2008, **160**, 576-581.
48. S. M. de Oliveira Brito, H. M. C. Andrade, L. F. Soares and R. P. de Azevedo, *Journal of Hazardous Materials*, 2010, **174**, 84-92.
49. D. Özer, G. Dursun and A. Özer, *Journal of Hazardous Materials*, 2007, **144**, 171-179.
50. H. Lata, V. K. Garg and R. K. Gupta, *Dyes and Pigments*, 2007, **74**, 653-658.
51. S. Zhu, S. Fang, M. Huo, Y. Yu, Y. Chen, X. Yang, Z. Geng, Y. Wang, D. Bian and H. Huo, *Journal of Hazardous Materials*, 2015, **292**, 173-179.
52. L. Fan, C. Luo, X. Li, F. Lu, H. Qiu and M. Sun, *Journal of Hazardous Materials*, 2012, **215–216**, 272-279.

Figures and Tables

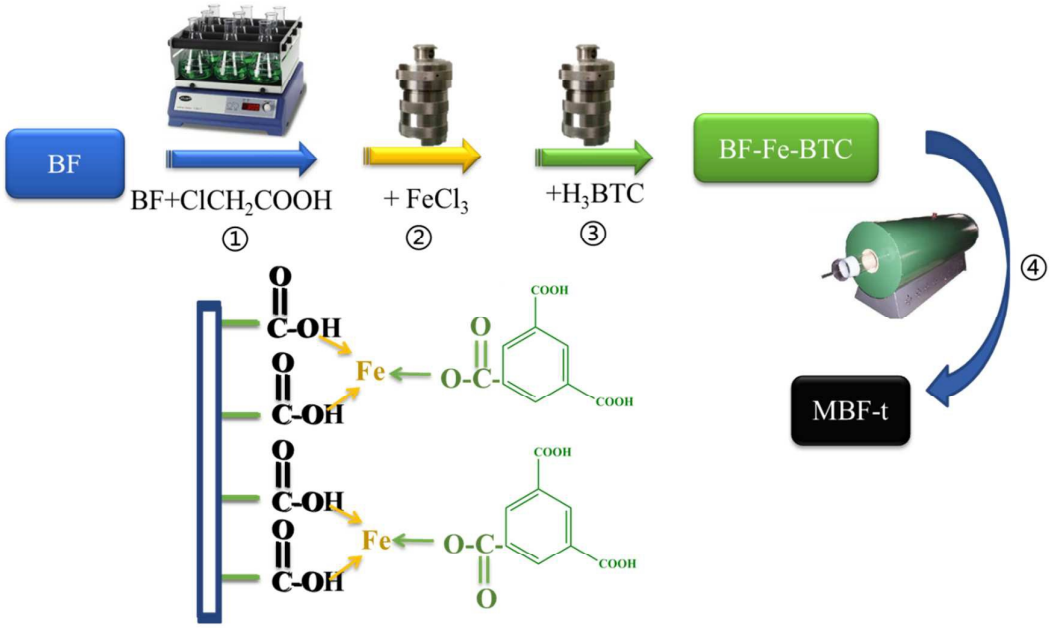

Fig. 1 Schematic illustration of the fabrication process of MBFs.

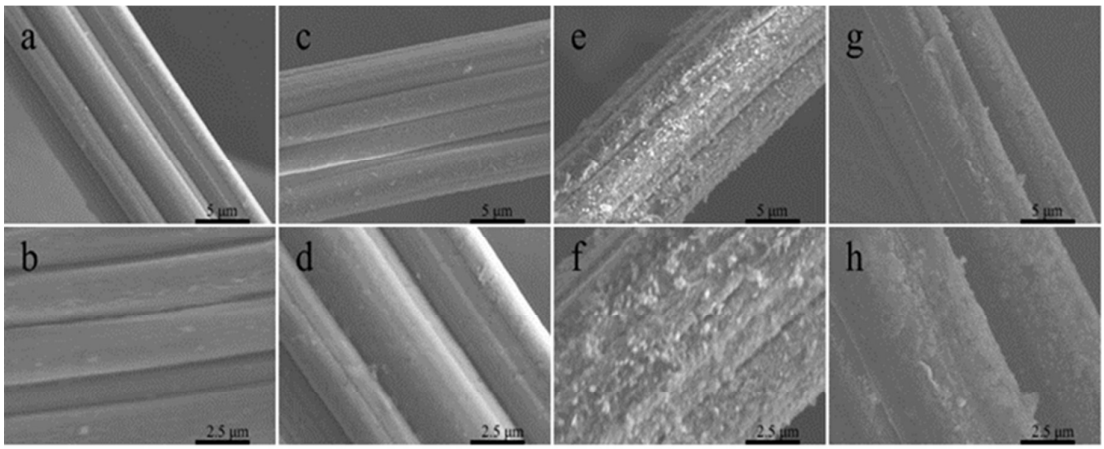

Fig. 2 SEM images of (a, b) bamboo fibers (BF), (c, d) BF-COOH, (e, f) BF-COOH-Fe^{3+}, (g, h) BF-Fe(BTC).

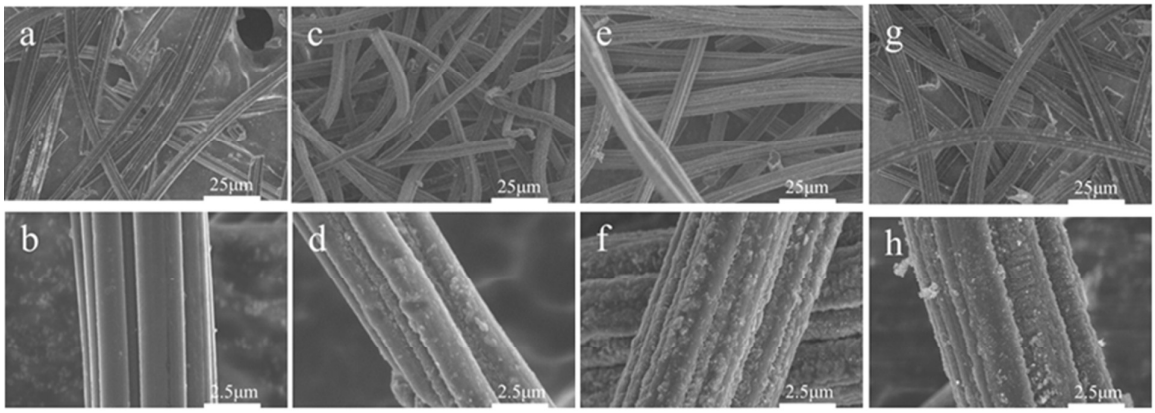

Fig. 3 SEM images of (a, b) CBF, (c, d) MBF-500, (e, f) MBF-700, (g, h) MBF-900.

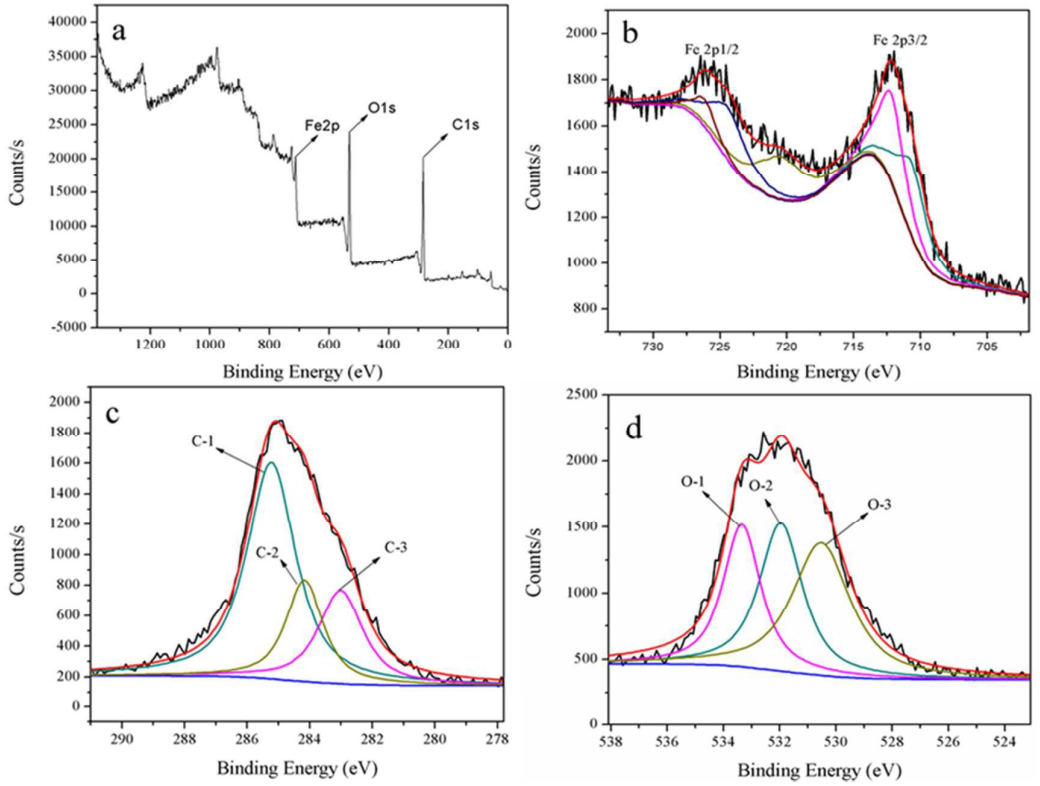

Fig. 4 shows the survey XPS data, indicating that MBF-900 contains the three elements Fe, O, and C.

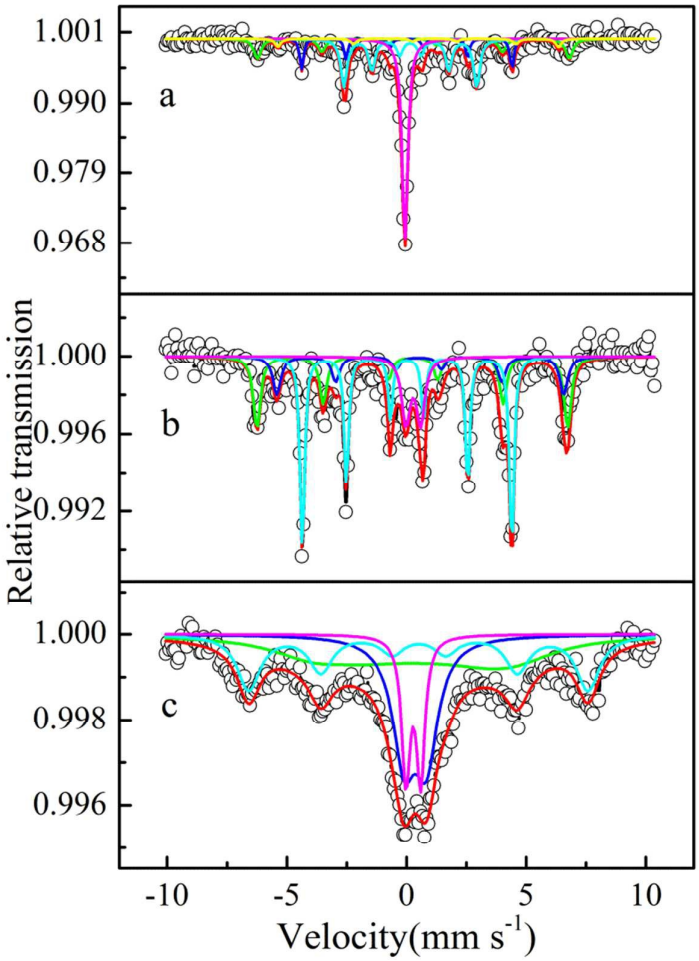

Fig. 5 MÖssbauer spectrum of (a) MBF-500, (b) MBF-700, and (c) MBF-900.

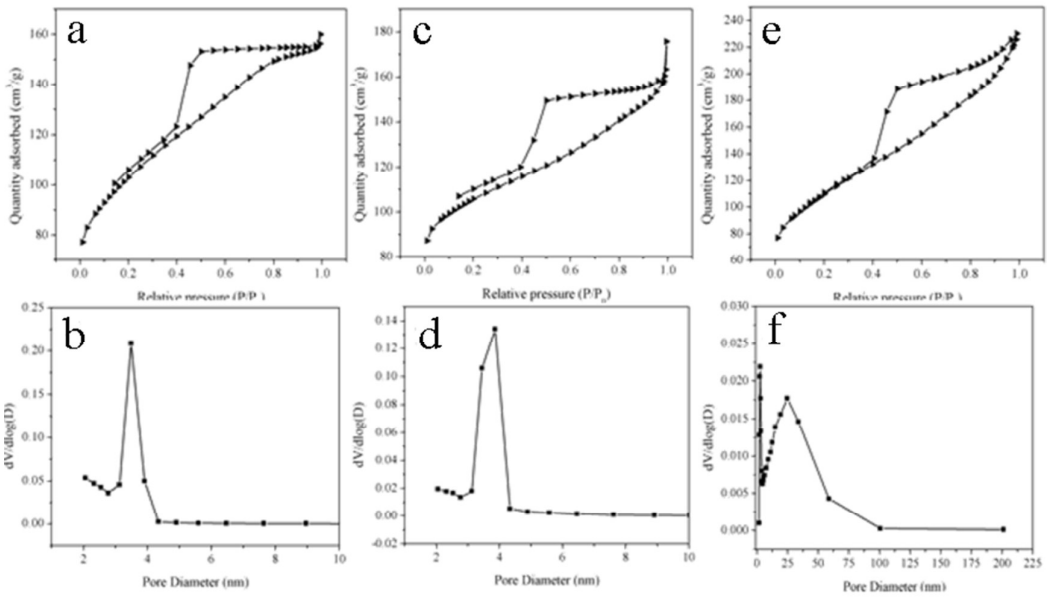

Fig. 6 N_2 adsorption-desorption isotherms of (a) MBF-500, (c) MBF-700, and (e) MBF-900. the pore-size-distribution curve of (b) MBF-500, (d) MBF-700, and (f) MBF-900 obtained from the desorption data through the BJH method.

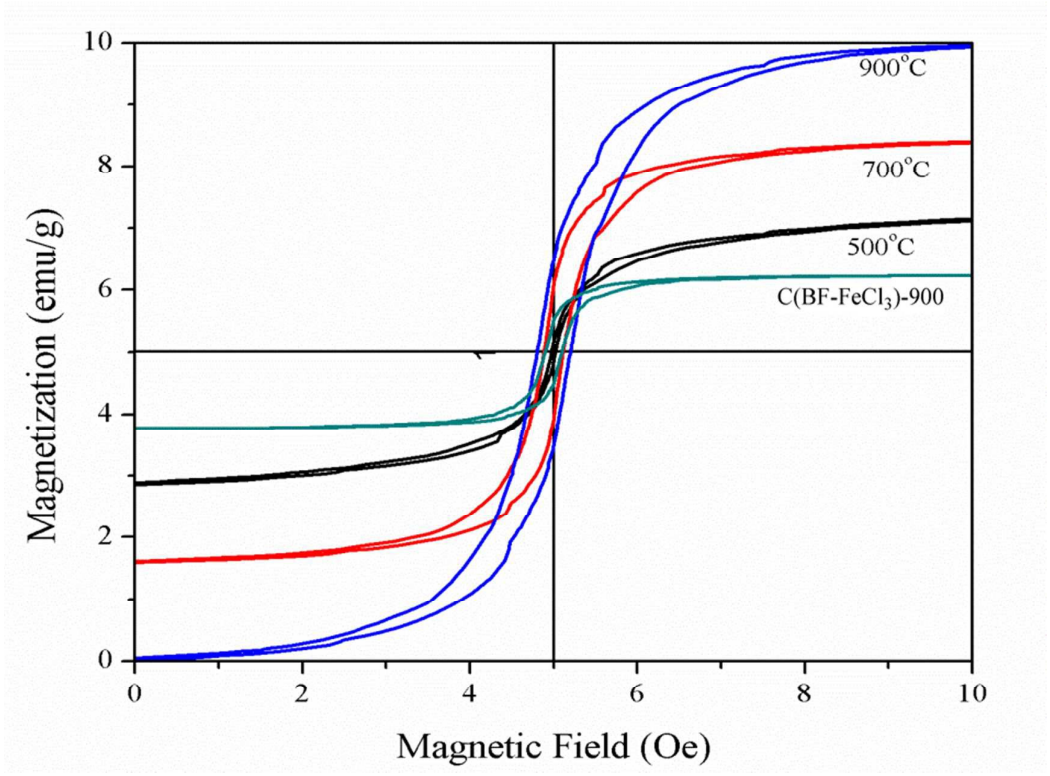

Fig. 7 Magnetic hysteresis loops of MBF-500, MBF-700, MBF-900, and C(BF-$FeCl_3$)-900.

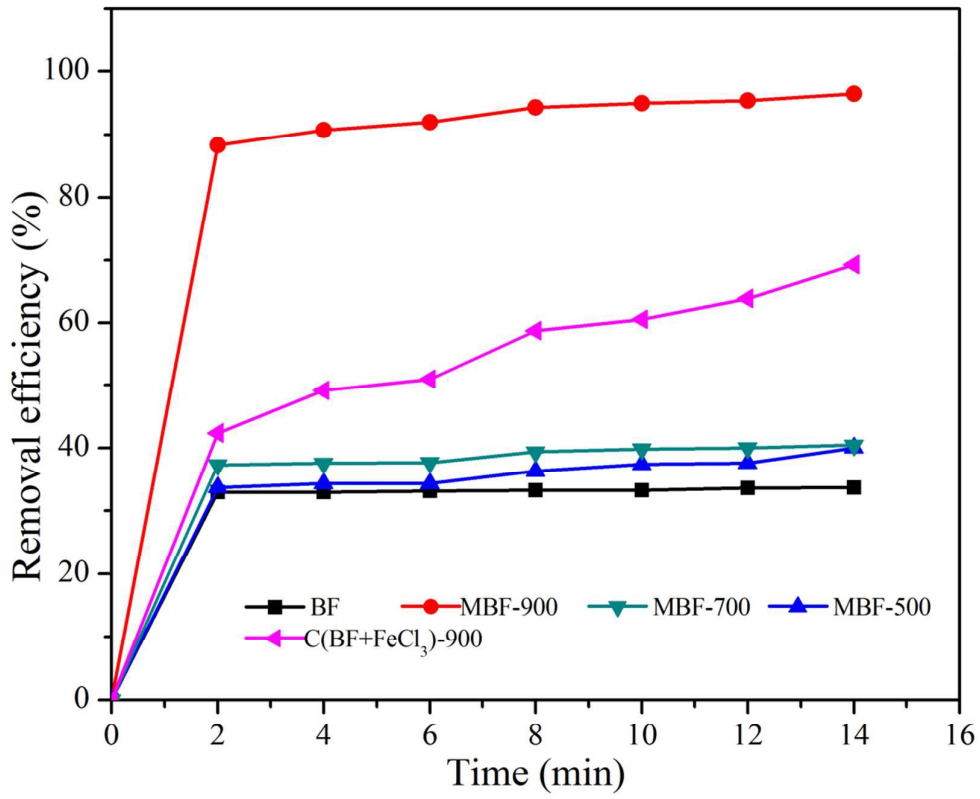

Fig. 8 Kinetic adsorption plots of BF, C(BF-$FeCl_3$)-900, MBF-500, MBF-700, and MBF-900 for MB plot of removal amount (Q_t) vs. time t. The initial concentration of MB solution was 60 mg/L and samples were 1 g/L.

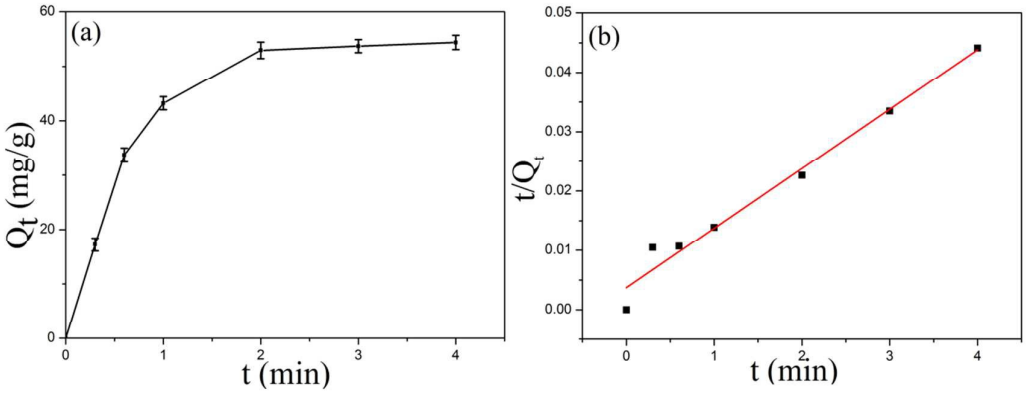

Fig. 9 Kinetic adsorption plots of MBF-900 for MB. (a) plot of removal amount (Q_t) vs. time t; (b) plot of pseudo-second-order kinetics for the adsorption process of the hybrid. The initial concentration of dye solution was 60 mg/L and MBF-900 was 1 g/L.

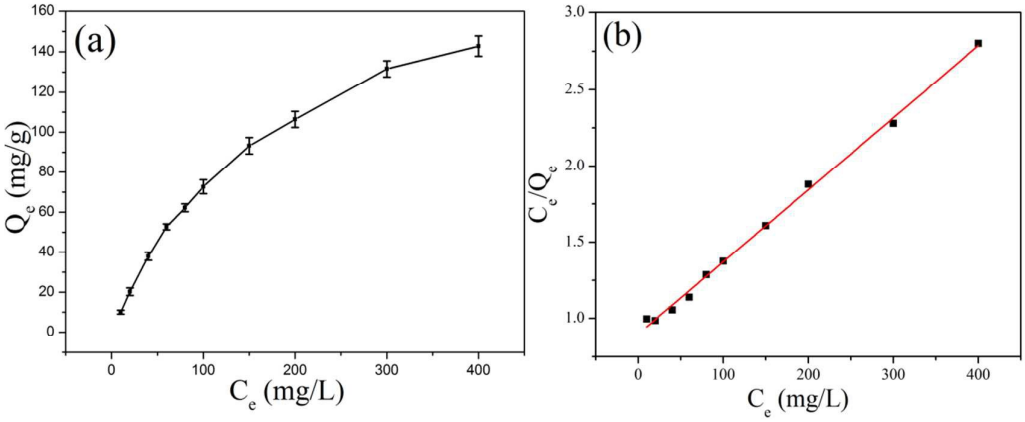

Fig. 10 Adsorption isotherms of MB onto the MBF-900 at 298 K (a) and the linear regression by fitting the equilibrium adsorption data with the Langmuir adsorption model (b)

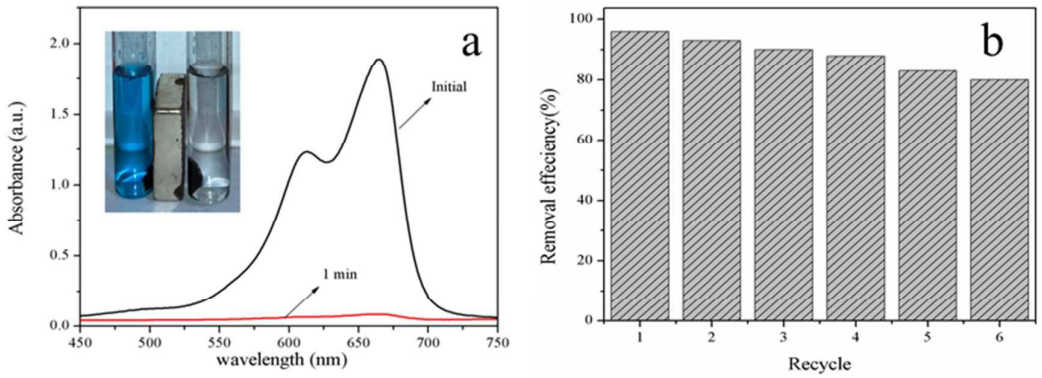

Fig. 11 (a) Time dependent absorption spectra of MB in the presence of MBF-900. The initial concentration of MB solution was 40 mg/L and samples were 1 g/L. The inset demonstrates MBF-900 could be separated from MB solution by a magnet. (b) The reusability of the MBF-900 for MB.

Table 1 BET surface area, pore volume and pore size of the MBF-500, MBF-700, and MBF-900.

Composites	Surface area (m^2/g)	Pore Volume (cm^3/g)	Pore Size (nm)
MBF-500	359.33	0.2392	2.66
MBF-700	360.72	0.2429	2.69
MBF-900	387.74	0.3394	3.50

Table 2 Magnetic Properties and Iron Content of C(BF-$FeCl_3$)-900, MBF-500, MBF-700, and MBF-900.

Samples	magnetic parameters			
	M_S (emu/g)	M_R (emu/g)	H_C (Oe)	H_m (Oe)
C(BF+$FeCl_3$)-900	0.86	0.38	241	1773
MBF-500	1.39	0.55	113	2853
MBF-700	2.58	1.17	366	4120
MBF-900	3.87	1.54	529	6653

Table 3 Pseudo-first-order, pseudo-second-order, Elovich equation, and Intraparticle diffusion model rate constants for the adsorption of MB on MBF-900 at 25°C

Elovich equation			Intraparticle diffusion model		
α	β	R^2	K_3	C	R^2
80.53	0.047	0.9698	16.01	6.18	0.8711
Pseudo-first-order kinetic model			Pseudo-second-order kinetic model		
q_e	K_1	R^2	q_e	K_2	R^2
40.83	0.60	0.8337	100	0.027	0.9739

Table 4 Langmuir and Freundlich parameters for the adsorption of MB on MBF-900 at 298 K.

Langmuir		
Q_m(mg/g)	K_1(L/mg)	R^2
143.0	0.0053	0.9971
Freundlich		
K_F((mg/g)(L/mg)$^{1/n}$)	1/n	R^2
0.24	1.40	0.9713
Temkin		
A	B	R^2
-92.75	37.60	0.9531

Table 5 Comparison of various adsorbents to remove MB.

Adsorbents	Adsorption capacity (mg/g)	Reference
BNS	7.81	[46]
Dehydrated peanut hull	108.6	[47]
Phosphoric acid treated	88.5	[48]
Prepared Fe_3O_4 MPs from iron	99.4	[49]
Magnetic chitosan	60.4	[50]
MBF-900	143.0	This work